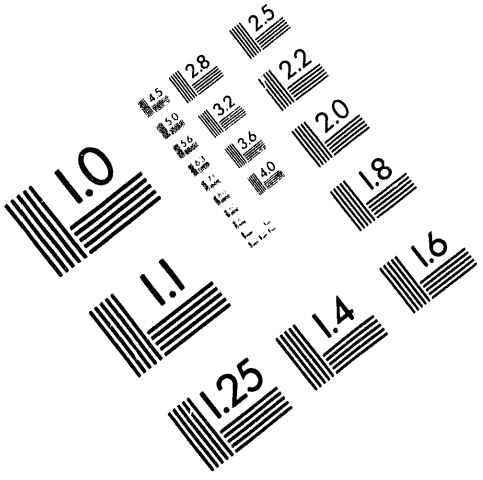

Association for Information and Image Management

1100 Wayne Avenue, Suite 1100
Silver Spring, Maryland 20910

301/587-8202

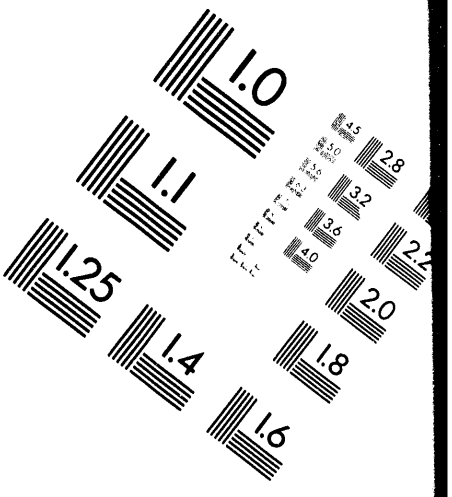

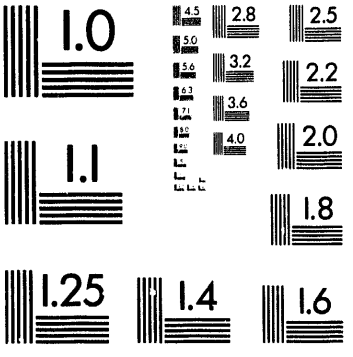

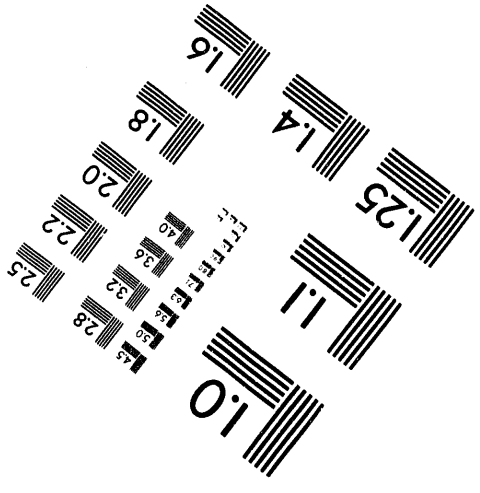

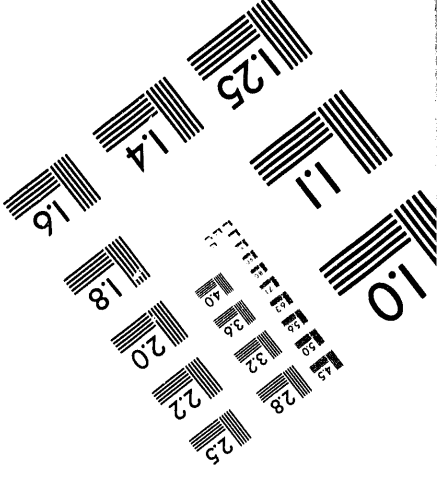

1 of 1

2

CONF-9410131--1

SAND-94-0081C

HVIS Paper No. 143

05/16/94

The Influence of Phase Changes On Debris-Cloud Interactions With Protected Structures

R. J. Lawrence,[a] L. N. Kmetyk,[b] and L. C. Chhabildas[c]

[a]Computational Physics Research & Development Department
[b]Thermal/ Hydraulic Analysis Department
[c]Experimental Impact Physics Department

Sandia National Laboratories
P.O. Box 5800
Albuquerque, New Mexico 87185 USA

Abstract

The physical state of the debris cloud generated by the interaction of a projectile with a thin target depends on the energy balance associated with the impact event. At impact velocities well above the sound speeds of the materials involved, the cloud is expected to be primarily molten, but with some vapor present. A series of numerical calculations using the multi-dimensional finite-difference hydrocode CTH has been used to evaluate the effect of phase changes (*i.e.*, different vapor fractions) on these clouds, and their subsequent interaction with backwall structures. In the calculations, higher concentrations of vapor are achieved by increasing the initial temperature of both the projectile and the thin shield while keeping the impact velocity constant, and by actually increasing the impact velocity. The nature of the debris cloud and its subsequent loading on the protected structure depend on both its thermal and physical state. This interaction can cause rupture, spallation, or simply bulging of the backwall. These computational results are discussed and compared with new experimental observations obtained at an impact velocity of ~10 km/s. In the experiment, the debris cloud was generated by the impact of a plate-shaped titanium projectile with a thin titanium shield.

This work was supported by the United States Department of Energy under Contract DE-AC04-94AL85000.

INTRODUCTION

The interactions that occur when hypervelocity projectiles impact targets can be categorized as either "thin target" or "thick target" depending on whether the target is penetrated. In the former case the projectile may penetrate without disintegrating, or it may, if the kinetic energy is great enough, breakup into solid, liquid, and possibly vapor constituents. For thick targets, crater formation, shock generation and propagation, possible target spall, and other related phenomena are of primary interest. However, it is the "thin-target" case that is being investigated here, in particular, for conditions where the hypervelocity projectile and the swept out portion of the impacted target form an expanding cloud of possibly multi-phase debris. This situation has important applications, ranging from the use of stand-off or "Whipple bumper" shields for the protection space-based assets from orbital and other debris, to the study of kinetic-energy lethality and vulnerability associated with the defense against strategic and tactical missiles.

The salient characteristics that these latter applications have in common include: 1) impacts at hypervelocities, which are generally considered to be above the sound speeds of the relevant projectile and target materials; 2) targets thin enough so that penetration occurs; 3) the formation of expanding debris clouds consisting of solid fragments, fluid droplets, and possibly vaporized materials; and 4) void spaces behind the initial layer that are large compared to the characteristic dimensions of either the projectile or the solid parts of the target. This last attribute allows the debris cloud to be "frozen out" for a considerable length of its then ballistic trajectory. In the present effort we will use the stand-off shield application to study the importance of the characteristics of the debris cloud on the response of the underlying backwall structure.

Stand-off shields for spacecraft applications were originally designed, somewhat empirically, to protect against micrometeoroids, which are typically 100-micron-size silicate particles with relative velocities as high as 20 km/s. With the increasing exploration of space over recent decades, this environment has expanded significantly to include various types of man-made orbital debris. The new threat includes irregularly shaped metallic particles with masses in the vicinity of a gram and diameters that range from millimeters to roughly a centimeter (larger particles can generally be detected and evaded). They will impact with average velocities of 10 km/s or more. Their average density is ~2.8 g/cm^3, and they are usually characterized with the material properties of aluminum. The requirements for these shields have thus become much more demanding, and in the absence of readily available experimental testing capabilities at the upper limit of the anticipated loading conditions, detailed and validated theoretical analyses are essential.

Within the last several years this problem has been addressed both experimentally and theoretically. Tests performed to evaluate the integrity of a single-layer bumper shield at impact velocities of ~10 km/s were conducted with parameters representing a current Space Station shield design.[1] The results indicated that a 0.6-g aluminum plate-shaped projectile generated a debris cloud capable of penetrating a hull structure

event. In addition we provide a brief description of the computational approach used for the analysis, employing the hydrocode CTH, and then give a detailed discussion of the other calculations performed as part of this study.

NEW EXPERIMENTAL OBSERVATIONS

The new stand-off shield experiment conducted as part of this study involved the use of a titanium projectile impacting a titanium shield at almost 10 km/s. The overall specifics of the experimental setup are described in detail elsewhere.[3] However, for this particular experiment, Shot No. XH-9, the flyer was a 1-mm thick, 12.7-mm diameter titanium alloy (Ti-6Al-4V) plate-like projectile impacting at 9.7 km/s. It had a mass of 0.53 g. The single-layer shield was 0.74 mm thick and was made of the same material. The simulated backwall structure was made of 4-mm-thick 6061-T6 aluminum and was located behind the shield at a stand-off distance of 150 mm.

Two principal diagnostic techniques were used to observe the debris cloud. They were: 1) fast framing photography; and 2) flash x-ray radiography. The framing photography collects light reflected, scattered, and radiated from the expanding debris cloud, whereas the flash x-ray images are exposed by x rays transmitted through the debris. For this reason, the photographs tend to be sensitive to the low density, hot vapor portion of the cloud, and the radiographs record the higher density material within the cloud. Combining these two complementary approaches yields a comprehensive set of image data that provides for reasonably complete characterization of the debris clouds. Figure 1 shows a schematic of the configuration employed by these diagnostics.

Both photographs and radiographs from Shot XH-9 are shown in Figure 2. The left-hand image in both rows is a flash x-ray radiograph of the projectile just before impact. It indicates that the flyer is intact but slightly bowed. In the center of the upper row is an x-ray image that was exposed at about 5.8 μs after impact. It is apparent that most of the debris mass is moving in three narrow columns all roughly parallel with the impact direction. In the center of the lower row is a framing camera photo, also recorded at a time of 5.8 μs. The central columnar streams of high-density material are not visible, but are obscured by diffuse clouds of low-density vapor, which dominate the picture. Note that the outer edge of the debris cloud in the photograph has propagated farther than that in the radiograph, indicating that the low-density vaporized debris is traveling faster than the higher-density material imaged by the x rays. Analysis of these images suggests that the vaporized leading edge of the debris is moving at over 11 km/s, while the x-ray radiograph yields a peak velocity of ~10 km/s. This is consistent with earlier results obtained with aluminum flyers impacting aluminum shields at similar velocities.[4,5] The x-ray images in the right-hand column of the figure, taken at about 15 μs, indicate that the debris cloud has sufficient momentum and energy to rupture the backwall structure. The penetration occurs on the centerline and appears to produces a hole with a diameter of a little over 3 cm.

DESCRIPTION OF NUMERICAL MODEL

The numerical calculations were performed with the Eulerian finite-difference hydrocode CTH.[6] In the present study we used two-dimensional cylindrical geometry, and employed nonequilibrium, multi-material temperature and pressure modeling options, along with the high resolution interface tracker. The velocities were convected, conserving momentum exactly and discarding any kinetic energy introduced by discrepancies in energy conservation. Artificial viscosity was used, with conventional default values for the linear and quadratic coefficients, and with the shear component increased somewhat. The regions around the flyer, the shield, and the backwall were modeled as voids.

The flyer plate, the bumper shield, and the backwall were all described thermodynamically with the ANEOS equation of state,[7] and were modeled mechanically as elastic perfectly-plastic materials. Table I provides a listing of the major properties for the actual materials involved in the baseline calculation.

Table I. Principal Properties for Materials in Baseline Calculation

	Titanium (Ti-6AL-4V)	Aluminum (6061-T6)
Density, ρ_o (g/cm^3)	4.42	2.70
Sound Speed, c_o (km/s)	4.99	5.32
Vaporization Energy, ε_v (kJ/g)	9.8	12
Grüneisen Parameter, Γ_o	1.09	2.06
Yield Strength, Y_o (GPa)	1.2	0.5
Poisson's Ratio, υ	0.32	0.33

The specific geometry for the baseline case is given in the previous section, and is summarized in Table II. Because of the large void region between the shield and the backwall (40 to 200 times the size of the other important characteristic dimensions of the problem), the debris cloud will be on a ballistic trajectory for a large portion of its flight path. To describe fully this motion with an Eulerian finite-difference code would require a very large number of spatial zones, and would consume a great deal of computer time, but would add little significant information to the calculated results. Hence these problems were run in two stages, emphasizing first the projectile impact on the shield, and then the impact of the debris on the backwall. In this fashion optimum resolution, both spatial and temporal, was provided in the regions where it was most needed. The first stage concentrated on the projectile impact and provided a detailed

description of the generation and initial evolution of the debris cloud. These numerical results were then mapped onto a different mesh, which was then used to examine the interaction of the debris cloud with the backwall.

Table II. Configuration for Shot No. XH-9

Impact Velocity		9.7 km/s
Stand-Off Distance		150 mm
Projectile	Material	Titanium (Ti-6Al-4V)
	Thickness	1 mm × 12.7 mm dia.
Shield	Material	Titanium (Ti-6Al-4V)
	Thickness	0.74 mm
Backwall	Material	Aluminum (6061-T6)
	Thickness	4 mm

Bumper Shield Impact. For the first-stage calculations, the impact of the flyer plate was modeled with relatively fine zoning. In the radial direction (x is the radial coordinate), the mesh was started at $x = 0$, where this then represents the axis of symmetry in the cylindrical geometry employed for the numerical analysis. In the axial direction (y is the axial coordinate), the mesh was started at $y = -0.5$ cm, with the initial contact surface between the flyer plate and the shield defined at $y = 0$. A 400 × 750 subgrid of 0.01-cm-square zones was used in a central interaction region. This provides a cylindrical volume 8 cm in diameter (the mesh is reflected about the axis of symmetry) and 7.5 cm in length. Note that this fine zoning covers only about half the 15-cm distance between the shield and the backwall. Outside this subgrid additional zones were allowed to grow in size at a rate of 5% in both the radial and axial directions.

Backwall Interaction. The stage-one calculations were terminated at the time the debris cloud had expanded to fill almost the entire 400 × 750 square-cell subgrid. For impacts at ~10 km/s this took typically ~6 μs. At this time the material distribution was rezoned and mapped onto a larger and coarser grid that included the backwall structure. As with the stage-one calculation the new radial mesh was started on the axis of symmetry, $x = 0$, and the new axial mesh was started at $y = -0.5$ cm. In contrast to the stage-one zoning, this mesh used a 100 × 474 subgrid of 0.04-cm-square zones, which represents an 8-cm-diameter and 19-cm-long interaction region. Again, zones outside this subgrid were allowed to grow in size at a rate of 5% in both directions. This second stage of the calculation was run until the backwall was either penetrated or distorted and its movement was essentially stopped.

More details of the problem setup, including complete listings of the required equation of state parameters, as well as the full code input listings for both stages of the baseline calculation are given in the technical report associated with the project.[8]

BASELINE RESULTS

The first calculation to be performed was set up to simulate the experiment described above. This baseline description will be used as a point of reference for the subsequent calculations. In Figure 3 we show the initial development of the debris cloud at times of 2, 4, and 6 μs after initial impact from the stage-one calculation. In these and subsequent debris-cloud plots, contour lines show order-of-magnitude density variations, and the density of dots gives a qualitative representation of the actual material density and distribution. A higher density core is evident in the cloud, especially at the later times. This central column-like structure has a diameter about equal to that of the original flyer plate, and is traveling axially at roughly the original impact velocity. Low density material is seen expanding at a higher velocity both laterally and axially from that core. The material interface lines indicate that the front half of the debris cloud consists of shield material, while the back half of the cloud is made up of residue from the projectile. The temperatures are highest along the axis, with the column of higher-density material generally above the vaporization temperature, and with most of the outer, lower density material above the melt temperature.

The records from Shot No. XH-9, given in Figure 2, show the debris at a time of ~5.8 μs. The photo shows the leading edge of the low-density cloud traveling at ≥11 km/s, while the radiograph indicates a velocity of ~10 km/s for the higher density core material. The numerical results, from Figure 3, predict that the low-density debris front ($\rho \geq 10^{-6}$ g/cm^3) is moving at ~12 km/s, and that the front of the core ($\rho \geq 10^{-1}$ g/cm^3) has a velocity of ≤11 km/s. Although these values are a little higher than the measurements, they do indicate reasonably good qualitative agreement.

The subsequent expansion of the debris cloud and its interaction with the aluminum backwall structure, from stage-two of the calculation, are illustrated in Figure 4. They show the debris cloud at times of 10 and 20 μs, along with a close-up view of the ruptured backwall structure at 35 μs. By this latter time the hole has stopped growing and the material has, for all practical purposes, ceased its motion. In fact, this was the criteria used for terminating the second stage of the calculation, both here and in the following problems. The calculated hole size is somewhat less than suggested in Figure 2, however there is some uncertainty associated with the interpretation of this quantity.

To complete the description of this calculation, we retrieved both the pressure and impulse loading produced on the backwall by the debris cloud. By monitoring several Lagrangian points embedded in the backwall, we can see how the loading decreases with increasing distance from the centerline. On the axis, the first pressure increase is observed at ~12.5 μs. At about 15 μs it peaks at 5.7 GPa (57 kb), and by 17 μs it is back down to below 1 GPa. This gives a FWHM pulse duration of almost 4 μs. As the radius

is increased the pressure pulses arrive a little later, and are of smaller amplitude, until by x = 0.6 cm the peak value is only 1.8 GPa (18 kb). By integrating these pressure profiles over time, we determine the impulsive loadings at the same points. These late-time impulses are plotted in Figure 5 as a function of radius from the centerline. The peak axial value is 13.8 × 10^3 kg/m-s (138 ktaps), and at the radius identified with the backwall hole size, x = 0.6 cm, is down to a little over 5 × 10^3 kg/m-s (50 ktaps). This latter value may be a useful criterion for backwall failure.

COMPUTATIONAL VARIATIONS

Using the baseline calculation as a reference, several additional calculations were performed as *gedanken* exercises. Their principal purpose was to address the concept that increases in the vapor content of the debris cloud alone will increase the effectiveness of these shields. To investigate the phenomenon directly we first repeated the baseline problem with everything the same except for the initial temperatures of the projectile and shield. In a second pair of variations, only the impact velocity was changed from the baseline conditions, to 20 and 30 km/s respectively. Finally, again using the baseline calculation as a point of departure, the shield material was changed first to plexiglass and then to cadmium. These two materials offered both lower and higher densities than the baseline titanium, but maintained a similar, relatively low melting temperature.

Initial Temperature Variation. To increase the vapor content of the debris cloud directly, we simply increased the initial temperature of the projectile and/or the shield to values just below the melt and vaporization points, as indicated in Table III. Note that for titanium we have T_{MELT} = 1943 K and T_{VAP} = 3533 K respectively. Not surprisingly, these calculations showed that increased initial temperatures lead to increased speeds and greater dispersions for the debris clouds, but with few significant differences between the "hot shield" and "hot" cases. More specifically, in the baseline calculation the projectile debris consists of about equal amounts of molten and vaporized material, whereas in the two intermediate temperature cases almost 60% of the shield debris is vaporized. For the "very hot" case over two-thirds of the shield debris is vaporized.

As a result of the greater dispersion, the loading on the backwall also decreases with increasing initial temperature. Recall that the peak on-axis pressure was 5.7 GPa for the reference case; for the two intermediate temperature cases it is ~2 GPa, while for the "very hot" case it is only a little over 0.5 GPa. It is also interesting that for the higher temperature variants, the peak pressures drop off much more slowly with radius.

Table III. Variation of Initial Temperature

Problem Description	Flyer Temperature	Shield Temperature
Baseline	300 K	300 K
Hot Shield	300 K	1923 K†
Hot	1923 K†	1923 K†
Very Hot	3513 K‡	3513 K‡

† 1923 K = T_{MELT} - 20 K ‡ 3513 K = T_{VAP} - 20 K

Since the impulses are simply integrals of these pressure histories, they also decrease with increasing initial temperature. The main effect is, however, to flatten out the curves of impulse versus radius. On the axis the impulse is reduced from almost 14×10^3 kg/m-s, through a little over 8×10^3 kg/m-s for the intermediate cases, to 7×10^3 kg/m-s for the highest temperature, although the latter value is still rising slowly at the final calculated time of 35 μs. The primary consequence of these reduced impulses is the suppression of backwall penetration for all of the higher temperature calculations. These cases do show late-time bulging, but this observation suggests that "heated" shields have the potential for stopping hypervelocity projectiles that would penetrate a shield at ambient conditions. However, this effect is due to the increased dispersion of the debris cloud and the consequent reduction in specific momentum delivered to the backwall. The increased vapor content of the debris is simply the mechanism for producing the greater degree of dispersion.

Impact Velocity Variation. We can also substantially expand the fraction of the debris cloud that is vaporized by increasing the impact velocity. To see the effects of this approach, the baseline conditions were varied by increasing this velocity to 20 and 30 km/s respectively. Because of the increased kinetic energy and momentum, the debris clouds move considerably faster than in the baseline problem. In fact, their velocities are generally proportional to the impact velocities. The loading on the backwall is also greater, but not strictly in proportion to the input velocity. The peak pressures arrive earlier, but for the 20-km/s impact they are only about 30 to 40 percent greater than those for the baseline case, while for the 30-km/s impact they average 3.5 times the baseline values.

The backwall impulse profiles, shown in Figure 6, indicate that the higher velocity impacts produce enough additional debris dispersion so that the 20- and 30-km/s cases produce backwall impulses that are more broadly distributed than the loads generated by the 10-km/s impact. Note however, that the pressure pulses show enough variation in duration to cause the impulse curves for the lower two impact velocities actually cross each other near the axis. With the extra momentum and energy associated with the

30-km/s impact, its impulse always lies well above the other two curves. Even though the higher velocity backwall impulses are somewhat less peaked on the centerline, their amplitudes are large enough to lead to penetration and rupture in all cases. The predicted hole diameters follow the impact velocities: ~1.3 cm for the 10 km/s baseline case; ~2.1 cm for 20 km/s; and ~3.1 cm for 30 km/s. Clearly the increased amounts of vapor produced by larger impact velocities do not suppress backwall failure. Increased vapor fractions *do* increase the dispersion, but they can not compensate for the greater momenta and kinetic energies (four and nine times the baseline for the latter) associated with these greater impact velocities.

Variation of Shield Material. Plexiglass and cadmium are two alternate shield materials that bracket the titanium alloy in density, but have similar and relatively low melt temperatures. For comparison with the other materials, their major properties are listed in Table IV. In these calculations, the shield thicknesses were adjusted to keep the areal densities constant. Where the titanium baseline shield was 0.74-mm thick, the cadmium shield was 0.37-mm thick, and the thickness of the plexiglass shield was 2.8 mm.

Table IV. Principal Properties of Alternate Shield Materials

	Cadmium	Plexiglass
Density, ρ_o (g/cm^3)	8.92	1.18
Sound Speed, c_o (km/s)	2.4	2.7
Vaporization Energy, ε_v (kJ/g)	1.3	2.0
Grüneisen Parameter, Γ_o	2.3	0.86
Yield Strength, Y_o (GPa)	0.5	0.1
Poisson's Ratio, υ	0.33	0.33

Neither of these other shield materials was able to suppress backwall failure under the baseline impact conditions. However, the pressure and impulse loading did vary among the three materials. For plexiglass the pressure pulse arrives at the backwall considerably earlier than with either cadmium or titanium. The amplitudes of these pulses do not differ by large factors; on the axis, all three are between 4.5 and 6 GPa, while at a radius of 0.6 cm they are all between 1.5 and 2 GPa. For the impulses, as shown in Figure 7, the cadmium shield consistently gives the highest values, peaking at over 17 × 10^3 kg/m-s on the axis, and dropping to 7 × 10^3 kg/m-s at 0.6 cm. The titanium curve is similar in shape, at about three-quarters of the amplitude. In contrast, the curve for plexiglass, which is below the others over most of the backwall, shows some structure, and even crosses the titanium curve at smaller radii. At diameters of

1.1 cm for the plexiglass shield, 1.3 cm for titanium, and 1.8 cm for cadmium, the backwall hole sizes roughly correlate with the shield densities.

CONCLUSIONS

The multi-dimensional Eulerian hydrocode CTH has been used to investigate the effects of phase changes on impact-induced debris clouds and their subsequent interaction with typical backwall structures. There has been considerable speculation that an increased concentration of vaporized material in these debris clouds would, in many situations, be sufficient to prevent backwall rupture. Clearly this concept of expanded vapor content as the primary factor responsible for increased stand-off shield effectiveness is overly simplistic. Many aspects of the problem such as the density and thermodynamic properties of the shield, the energy partitioning and divergence of the debris cloud, and the actual geometry and properties of the backwall, must also be considered in detail.

To study some of these phenomena we first used the code to simulate a representative stand-off-shield experiment conducted at an impact velocity of ~10 km/s. This calculation, which agrees qualitatively with the observations, was then used as a baseline to look at several excursions from the nominal conditions. The vapor content of the debris cloud was increased, first by raising the initial temperature of the shield to values just shy of the melting and vaporization points, and then by boosting the impact velocity by factors of two and three. Other, relatively low melting point shield materials were also examined. The only variation that succeeded in eliminating backwall rupture was the increase in initial temperature. The other examples all contained additional factors, such as greater kinetic energy and momentum, that swamped the desired combined effects of increased vapor content, expanded debris dispersion, and lowered impulsive loads on the backwall.

In general, we found that backwall penetration and rupture seemed to correlate most closely with the delivered impulse or specific momentum. Because it is an integral-like quantity, changes in impulse are less dependent on the problem details than are changes in non-integral variables such as pressure. In fact, models have been proposed that predict both backwall failure and extent of failure in terms of simply calculated impulse.[9] Although we haven't pursued the approach, comparison of the results of applying that model with the present calculations could increase our understanding of the phenomena involved, and it could also provide additional tools for the analysis and design of stand-off shields.

Optimized design of these shields still has many uncertainties, and the related phenomenology must be more fully evaluated both experimentally and theoretically. To conclude, we note that experimental capabilities are now becoming available that will allow testing over almost the entire range of orbital debris threats.[10] However, experiments using these capabilities are expensive, and the various theoretical approaches, both numerical and analytical, will still be required for full understanding and application of the phenomenology associated with successful shield functioning.

REFERENCES

1. L. C. Chhabildas, E. S. Hertel, and S. A. Hill, "Whipple Bumper Shield Results and CTH Simulations at Velocities in Excess of 10 km/s," *Int. J. Impact Engng*, Vol. 14 (1993).

2. R. J. Lawrence, *A Simple Approach for the Design and Optimization of Stand-Off Hypervelocity Particle Shields*, AIAA Paper No. 92-1465, AIAA, Washington, DC (1992).

3. L. C. Chhabildas and M. B. Boslough, "Experimental Technique to Launch Flier-Plates Representing Orbital Debris to Hypervelocities," *Proceedings, 1993 SPIE Conference*, Orlando, Florida, April 1993 (to be published).

4. L. C. Chhabildas, E. S. Hertel, and S. A. Hill, "Whipple Bumper Shield Tests at Over 10 km/s," *Shock Waves in Condensed Matter—1991*, S. C. Schmidt *et al.*, Eds., Elsevier Science Publishers B.V., Amsterdam (1992).

5. L. C. Chhabildas, E. S. Hertel, and S. A. Hill, "Experimental and Numerical Simulations of Orbital Debris Impact an a Simple Whipple Bumper Shield," *Proceedings of the Workshop on Hypervelocity Impacts in Space*, J. A. M. McDonnell, Ed., University of Kent, Canterbury (1991).

6. J. M. McGlaun *et al.*, *A Brief Description of the Three-Dimensional Shock Wave Physics Code CTH*, SAND 89-0607, Sandia National Laboratories, Albuquerque, NM (July 1989).

7. S. L. Thompson, *ANEOS Analytic Equations of State for Shock Physics Codes Input Manual*, SAND 89-2951, Sandia National Laboratories, Albuquerque, NM (March 1990).

8. L. N. Kmetyk *et al.*, *Effect of Phase Change in a Debris Cloud on a Backwall Structure*, SAND 93-????, Sandia National Laboratories, Albuquerque, NM (1993).

9. R. J. Lawrence, "Analytic Models for Hypervelocity Particle Shield Analysis," *Shock Compression of Condensed Matter—1993*, S. C. Schmidt *et al.*, Eds., Elsevier Science Publishers B.V., Amsterdam (1994).

10. L. C. Chhabildas, Private Communication, Sandia National Laboratories, Albuquerque, NM (1994).

FIGURE CAPTIONS

Figure 1. Schematic of experimental setup.

Figure 2. Experimental results from Shot No. XH-9. The projectile is imaged on the left, the debris cloud is shown in the center, and the penetration of the backwall is indicated on the right. The upper debris-cloud picture shows an x-ray radiograph, while the lower shows a framing camera photograph. The other views are all x-ray records.

Figure 3. Numerically produced images of the debris cloud for stage one of the baseline calculation. The times are measured from the initial impact of the flyer plate on the shield and are shown for (a) 2 μs, (b) 4 μs, and (c) 6 μs.

Figure 4. Debris cloud images for stage two of the baseline calculation. At 10 μs (a) the debris cloud has not reached the backwall; by 20 μs (b) the backwall has shown considerable motion and distortion; and at 35 μs (c), at the end of the problem, a close-up shows the ruptured backwall.

Figure 5. Late-time impulse distribution on backwall for baseline calculation. The peak value on the axis, 13.8×10^3 kg/m-s (138 ktaps), decays to a little over 5×10^3 kg/m-s (50 ktaps) at a radius of $x = 0.6$ cm. Note that this latter point is the approximate location of the edge of the hole produced by the debris cloud.

Figure 6. Variation of late-time impulse distribution on backwall with impact velocity. Because of the greater dispersion of the debris cloud, the 20-km/s impact actually produces a lower axial impulse than that for the baseline conditions. However, with nine times the kinetic energy of the baseline case, the 30-km/s impact yields significantly greater impulse loading at all radii. All three cases lead to backwall rupture.

Figure 7. Comparison of late-time impulse distribution on backwall for different shield materials. The profiles for cadmium and titanium are similar in shape, whereas the plexiglass shows more structure, even crossing the titanium curve near the centerline. All are sufficient to cause backwall rupture.

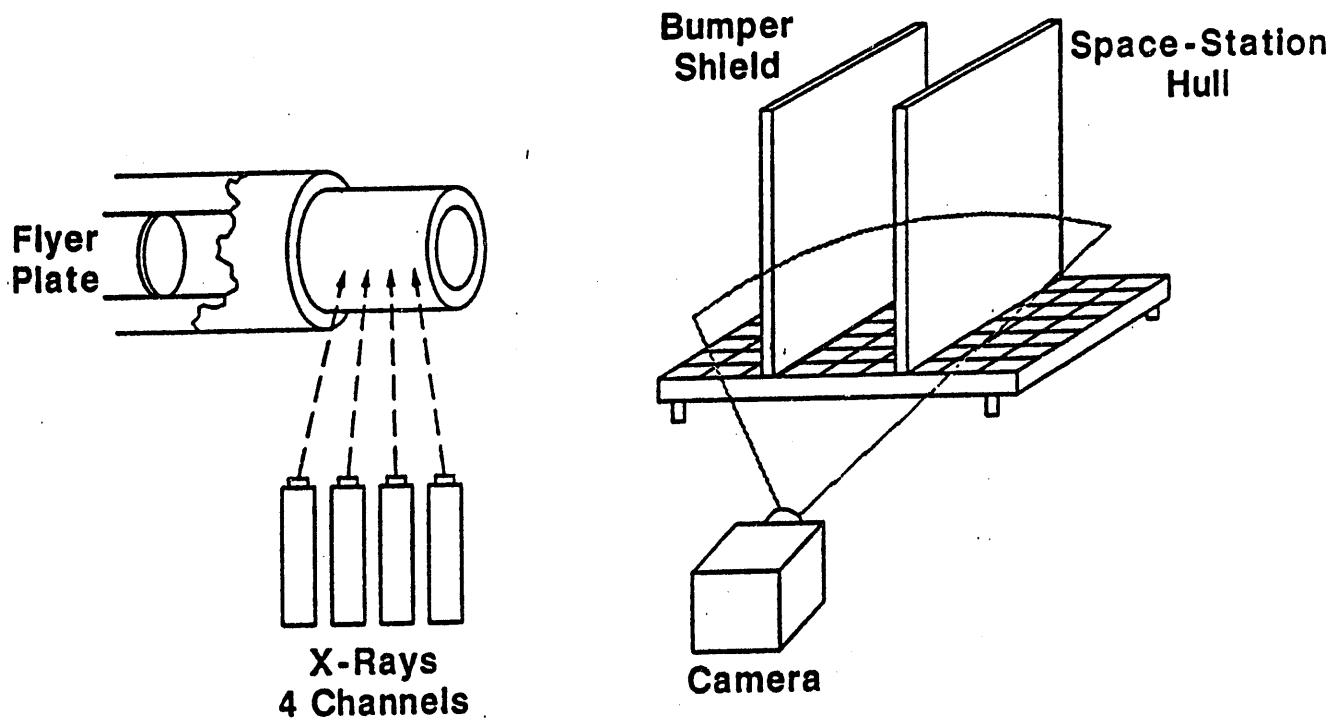
Bumper
Shield
Space-Station
Hull
Flyer
Plate
X-Rays
4 Channels
Camera

Fig. 1

Fig. 2

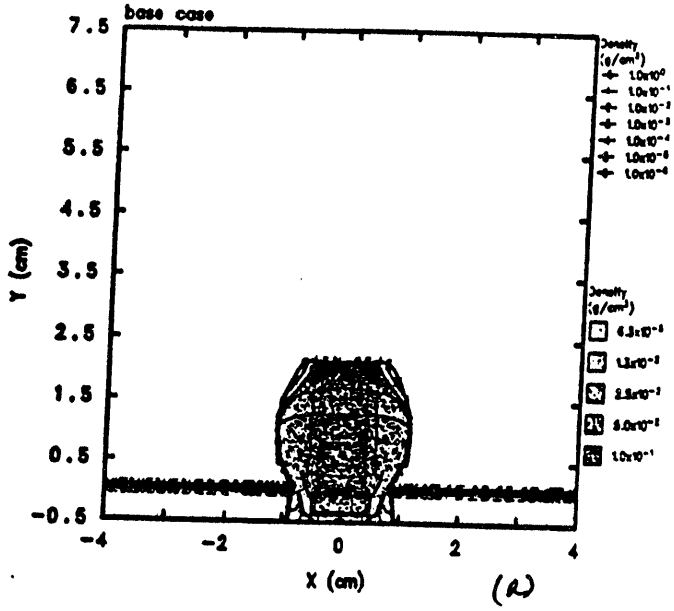

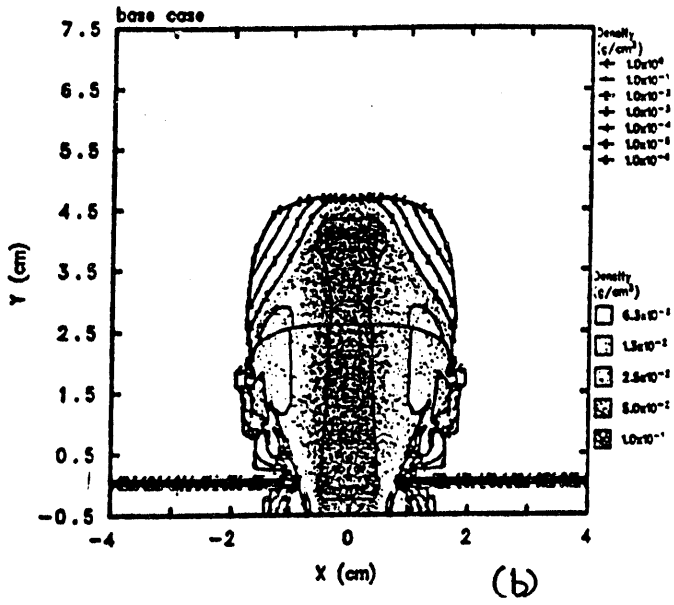

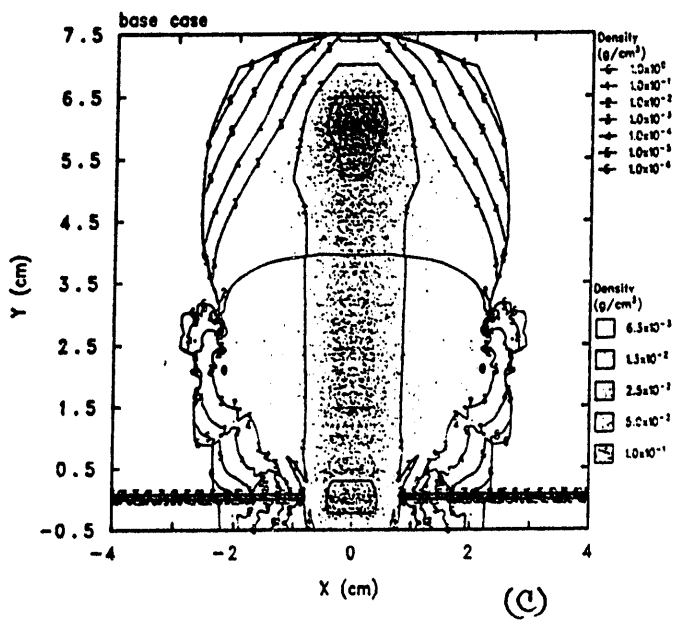

Fig. 3

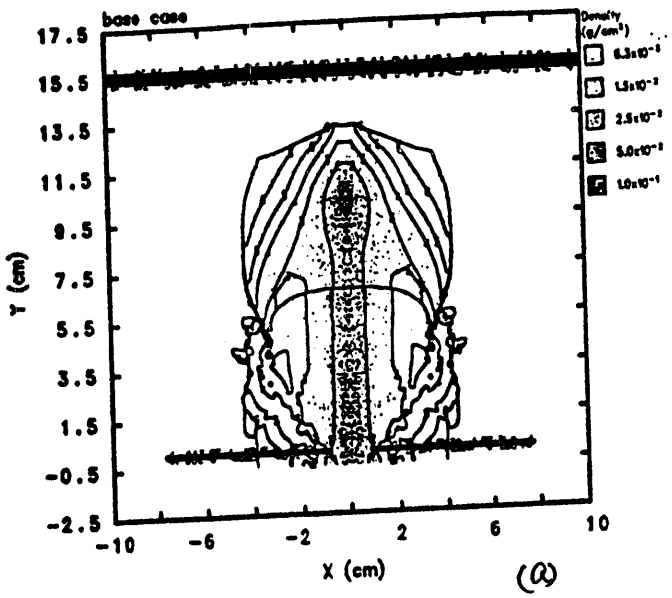
base case
Density (g/cm³)
Y (cm)
X (cm)
(a)

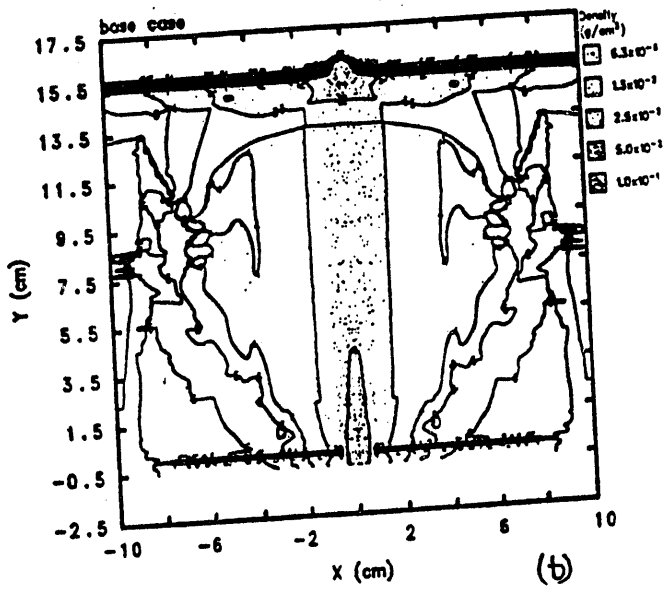
base case
Density (g/cm³)
Y (cm)
X (cm)
(b)

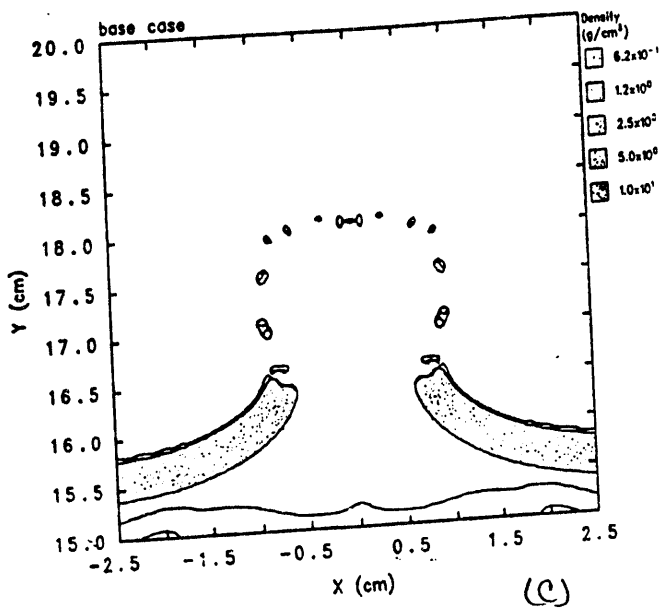
base case
Density (g/cm³)
Y (cm)
X (cm)
(c)

Fig. A

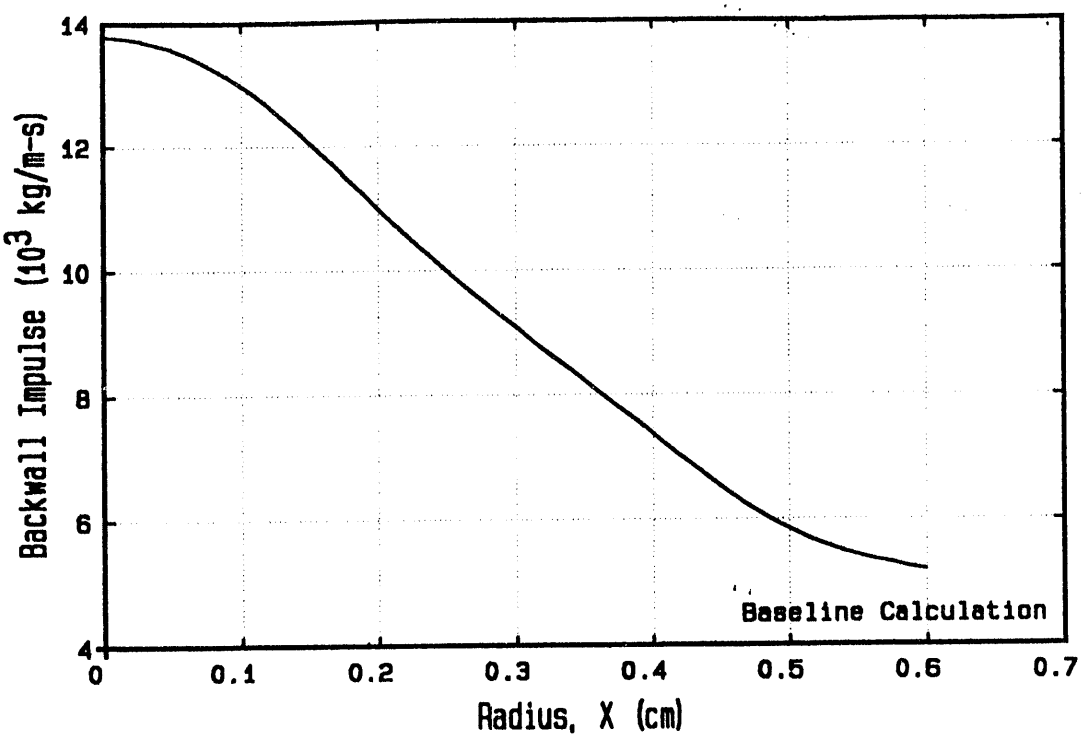
Backwall Impulse (10^3 kg/m-s)
14
12
10
8
6
4
0
0.1
0.2
0.3
0.4
0.5
0.6
0.7
Radius, X (cm)
Baseline Calculation

Fig. 5

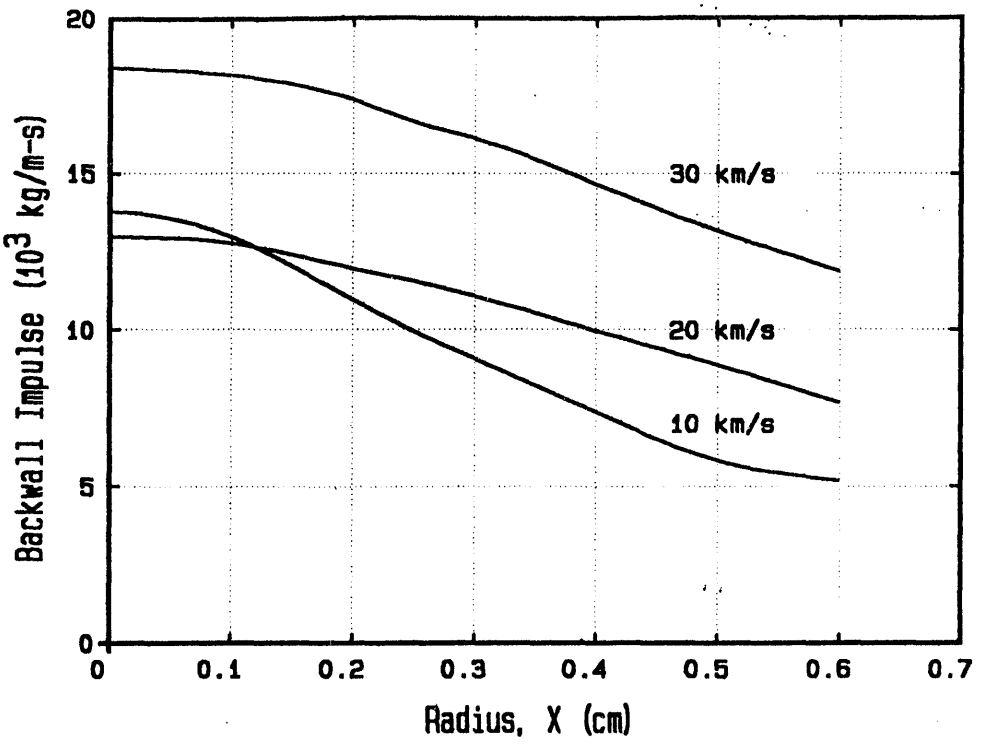
Backwall Impulse (10^3 kg/m-s)
20
15
10
5
0
0
0.1
0.2
0.3
0.4
0.5
0.6
0.7
Radius, X (cm)
30 km/s
20 km/s
10 km/s

Fig. 6

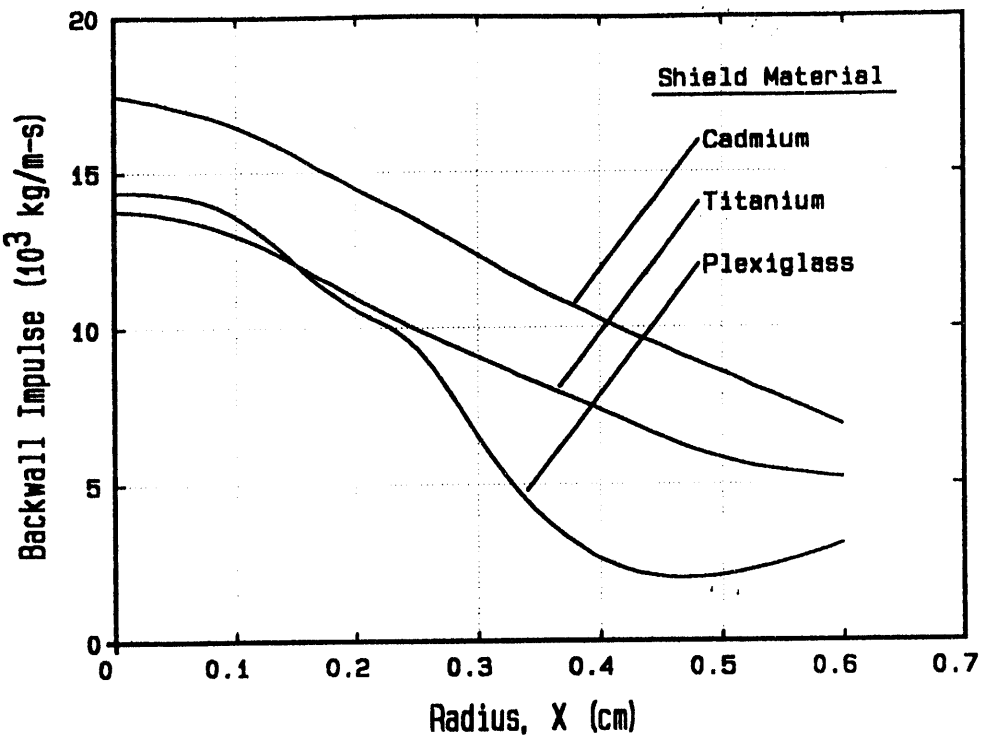
Shield Material
Cadmium
Titanium
Plexiglass
Backwall Impulse (10^3 kg/m-s)
Radius, X (cm)
0
5
10
15
20
0
0.1
0.2
0.3
0.4
0.5
0.6
0.7

Fig. 7

DATE
FILMED
9/8/94
END